E. Callone, S. Dire', X. Hu, A. Motta.

Processing influence on molecular assembling and secondary conformations in silk fibroin: elucidation by solid state NMR.

ACS Biomaterials Science and Engineering, 25, 758-767, 2016

DOI: 10.1021/acsbiomaterials.5b00507

Processing influence on molecular assembling and structural conformations in silk fibroin: elucidation by solid state NMR

AUTHOR NAMES. E. Callone[1,3], S. Dire'[1,3], X. Hu[5], and A. Motta[1,2,4]

AUTHOR ADDRESS.

1. Department of Industrial Engineering, University of Trento, Via Sommarive 9, 38123 Trento, Italy

2. BIOtech Research Center, University of Trento, Via delle Regole 101, 38123 Mattarello (TN), Italy

3. "Klaus Mueller" Magnetic Resonance Laboratory, Department of Industrial Engineering, University of Trento, Via Sommarive 9, 38123 Trento, Italy

4. European Institute of Excellence on Tissue Engineering and Regenerative Medicine, Trento Unit, Italy

5. Department of Physics & Astronomy, Biomedical & Translational Sciences, Biomedical Engineering, Rowan University, 201 Mullica Hill Road, 08028 Glassboro, New Jersey, USA

ABSTRACT

This study is devoted to the deep evaluation of processing-induced protein conformation changes by using silk fibroin fibers and their cast films stabilized by different methods as a model. The control of the hierarchical assembling of silk fibroin is the key for finely tuning the biological functions and physical-chemical properties of the final materials for applications in biomedical fields. However, previous methods usually only focused on the change of beta-sheet crystallinity in silk materials, which can not explain a lot their specific prosperities generated from different processing methods. By using complementary solid-state NMR, together with FTIR and DSC techniques, we first time established the correlations between processing conditions and silk fibroin molecular configurations, and experimentally assess the presence and quantify the percentage of the asymmetric three-fold helical conformation (Silk III) in silk materials, together with their well-known Silk I-like helix/coil dominated and Silk II beta-sheet dominated configurations. This work provides a roadmap for researchers to quantify the percentage of different silk structures by solid NMR, and further understand how silk molecular conformations (Silk I-like, II, III) can impact the properties and functions of different silk materials, that are broadly used today for different biomedical applications.

KEYWORDS: Solid state NMR, Processing, Silk Fibroin, FTIR, Secondary conformation, three-fold helix

1. INTRODUCTION

Silk fibroin-based materials have attracted a great attention as bioactive substrates for biomedical applications, such as tissue engineering, drug storage and delivery, biosensors and nanomedicine.[1-3] The ability of fibroin to favorably interact with biological systems and the advantages of fibroin scaffolds to engineer the repair and regeneration of different types of tissues were demonstrated by a large number of *in vitro* and *in vivo* studies.[4-6] Pre-cell seeded or unseeded scaffolds have been successfully tested for soft and hard tissues repair, in the form of gels, sponges, fibers or films, adapted to a several repair sites.[7-9]

Like other natural polymers, silk has a complex hierarchical structure that is assembled from the bottom-up, where its different conformations can be correlated to specific biological functions and physical properties. In general, *B. mori* silk fibroin is a structural protein, with a supramolecular structure composed by a Heavy-chain (about 350 KDa) linked to Light-chain (about 25 KDa) by a disulphide bound and correlated by a fibrohexamerin chain, P25, (about 20 KDa) in the ratio 6:6:1.[10] Silk fibroin Heavy-chain, results in a polypeptide chain of 5,263 residues, composed of glycine (45,9%), alanine (30,3%), serine (12,1%), tyrosine (5,3%) valine (1,8%), and 4,7% of others 15 amino acids, with a co-block polymer design. The crystalline forming regions of repeating peptide GAGAGX, where X is Ala in 65%, Ser in 23%,and Tyr 10%,[11] along the protein chain are connected by 11 less ordered sequences (GAGAGY) or/and AGVGYGAG blocks.[12] The dominant secondary conformation of silk fibroin can change depending on the microenvironment of the protein. Silk I is alpha-helix and coils dominated structure assumed by the protein in the silkworm silk glands just before the spinning,

characterized by a "liquid crystal" form, and it is water soluble.[13] Conformational transition is induced during the cocoon fiber spinning, and silk I is partially converted into a semi-crystalline structure comprising about 55% of β-sheet (silk II) structures embedded in an amorphous and hydrophilic matrix.[14] Alpha-helices conformation and intermediates structures, such as β-turns and β-bends, which can be ~~easily~~ recognized by FTIR-ATR,[15] could still remain in silk after the spinning due to the incomplete conversion to the β-sheet structure. Through a regeneration procedure, [16] silk fibroin fibers can be dissolved into aqueous solution and cast as soluble "silk I-like" films. It should be noted that the regeneration processing of silk fibroin can obtain significant amount of soluble helix structures in the final film sample, but may not be pure alpha-helix. Moreover, they may not be perfect silk I structures like those in the natural solution of silkworm glands. Asakura *et al*. well described the difference between silk I in the gland and the silk-I like structure formed in the man-made silk fibroin materials. [17] Here we used "silk I-like" to refer to the soluble helices/coil dominated structures in the regenerated silk samples. Most importantly, another conformation, detected in the ultra-thin silk fibroin film at air-water interface, was also found as the silk III, "*a threefold helical model crystal structure*". [6] The molecular structure model is proposed by Valluzzi *et al*.,[16] where the threefold helix, formed by the exapeptide GAGAGS, places all the serine residues on the same side of the structure, promoting an insoluble lamellar crystals formation, and is different from the beta-sheet crystals in Silk II. It need to be noted that, some of previous studies also called this structure "insoluble Silk I",[18] but in this study, we will uniformly call this insoluble structure Silk III to avoid additional controversy. In general, beta-sheet crystal dominated Silk II structure excludes water and is the most stable polymorph of silk fibroin in several solvents including mild acid and alkaline environments. While insoluble threefold helix conformation (silk III) gaps the

hydrophilic serine residues from the hydrophobic alanine residues, also playing a role in protein-water coordination and in the three-dimensional macromolecule assembling.

NMR experiments applied to fibroin fibers have been exploited in the last 30 years with great success.[19] The extended work of the research group of Prof. Asakura, through liquid and solid state NMR experiments, has ranged over the structural characterization,[20, 21] chain dynamics with NOE experiments,[22] and conformational studies based on 1D or 2D experiments on ^{13}C or ^{15}N nuclei.[23-25] A lot of experiments were made on regenerated fibroin produced by different sources, such as various silkworms or spiders,[19-22,26-29] driven by the fact that they show different mechanical properties. Most of these high quality NMR data were obtained through feeding the organisms with isotopically labeled aminoacids or sugars. Moreover, detailed information comes from the *ad hoc* preparation of isotopically labeled synthetic peptides with the aim of acquiring high quality ^{13}C and ^{15}N solid state NMR spectra and creates a panel of possible comparison with the above discussed natural samples.[30-35]

Starting from the pioneering work of Asakura, other researchers also investigated the sensitivity of fibroin conformations to synthesis, processing or environmental conditions. Many studies have been devoted on regenerated fibroin,[19,27-36] and also on electrospun fibers,[37] on the film obtained by casting[25,38-39] or even on spongy materials.[40] As a matter of fact, it has been demonstrated that solvent[41] and pH variations[25] or the presence of divalent/trivalent metal ions, such as Fe^{2+}/Fe^{3+}, at different concentration[38] in the fibroin dissolution step appear to affect the fibroin secondary structures, resulting in weak changes in position and line-shape of the NMR resonances at the solid state. However, no comparative evaluations between different silk

samples specifically designed for different tissue engineering applications were discussed previously. In fact, it is found not only the manipulation of fibroin solution affects the structure formation (different degumming protocols and stabilization methods), but also all the processing steps to produce fibers, films or composites should be taken into account. In the past, the focus was mainly on the mechanism of the structural transition during the natural fiber formation, and on assessing the structural difference of silk fibroin before spinning (silk I) and after spinning (silk II).[33,37,43] In addition, there is still a lack of an accurate method to quantify different secondary or supermolecular structures in a specific silk material in the past. Infrared and Raman spectra were used to quantify the contents of different silk structures in silk samples [12], but these methods could not identify and quantify many specific supermolecular structures in silk materials, such as insoluble triple-helix structures from silk III. However, considering that silk fibroin is a large fibrous protein, FTIR-ATR peaks shift can be affected by intermolecular interactions due to the protein segments rearrangement.[44] Accordingly, the solid state NMR analysis, successfully applied to the conformational studies previously, is here proposed together with infrared spectroscopy and differential scanning calorimetry, with the aim of first time quantifying the accurate contents of different secondary or supermolecular structures in fibroin film materials, which were fabricated from different conditions and in comparison with fibers and lyophilized powders. Here, fibroin films were used as an example of real tissue engineering scaffolds (i.e. for cornea regeneration,[45], sensors,[46] and optics,[47] and this quantitative method can be further applied to other forms of silk materials such as foams, particles or fibers. Depending on the specific application, fibroin films can be also fabricated by changing solvents, casting temperature, or protein concentration in the future. Natural degummed silk fibers and freeze-dried regenerated fibroin are intermediate products during process, thus were used as

comparative samples in this study. It appears that the processing could drive not only simply the Silk I/ Silk II ratio, but also the contents of many other conformations such as distorted β-turns, distorted β-sheets, β-sheets with parallel or alternating Ala CH_3, helix-like structures, random coils as well as the presence of the insoluble Silk III threefold helixes[16]. Self-assembly and the resulting conformation of these silk structures would in turn affect the physical behaviors of the materials,[21,48] and their biological outcomes[42]. Therefore, there is a need to use high-resolution structural analysis methods, such as NMR, to identify and quantify these different structures in silk materials in detail. With this information, conformational transitions from Silk I like soluble helix/random coil structures to silk II, or to intermediate β-strands and insoluble silk III structures therefore can be quantitatively calculated and modulated in silk materials. And functional design of materials based on this structural analysis would play an important role in fine-tuning the biological properties of silk fibroin-based devices in the future.

2. MATERIALS AND METHODS

2.1 Materials. *Bombyx mori* silkworm cocoons obtained from tetra-hybrid a Japanese female (79 x 71) (125 x 126), were kindly provided by Honey bee and Silkworm Research Unit, Padua seat, Council of Research and Experiments in Agriculture, Padova, Italy. All chemicals used were of analytical grade.

2.2 Preparation of silk fibroin water solution. All silk fibroin samples were prepared following the same standard protocol.[9] The silkworm cocoons were boiled in an aqueous solution of 0.02 M Na_2CO_3 twice for 90 min each, and then rinsed thoroughly with DI water to completely remove sericins. After air-drying at room temperature, the degummed silk fibroins

were dissolved in 9.3 M LiBr solution at 65 ºC for 4 h to produce 10% w/v silk fibroin solution. The silk fibroin solution was then dialyzed against deionized water using cellulose membrane (Pierce, MWCO 3,500) at room temperature. The concentration of the obtained aqueous silk fibroin solution is about 2.5% w/v, calculated by Nanodrop.

2.3 Films preparation. Films were prepared by solution casting, starting from a fibroin water solution 2.5%wt and then air-drying at room temperature. The dried films (sample CF) were then treated with 80% v/v methanol for 10' at room temperature (sample CF_{MeOH}), and in water vapor under vacuum in a desiccator (annealing process) for 24 hours at room temperature (sample CF_{WV}) to induce conformational change of silk fibroin. Films stabilized by methanol treatment and annealing was compared with untreated samples (CF), lyophilized fibroin after dialysis (LYO), and degummed silk (native fibroin) (DS). The complete procedure used for obtaining the different samples is described in Figure 1. All samples were prepared by using the same batch solution and stored at room temperature in desiccator.

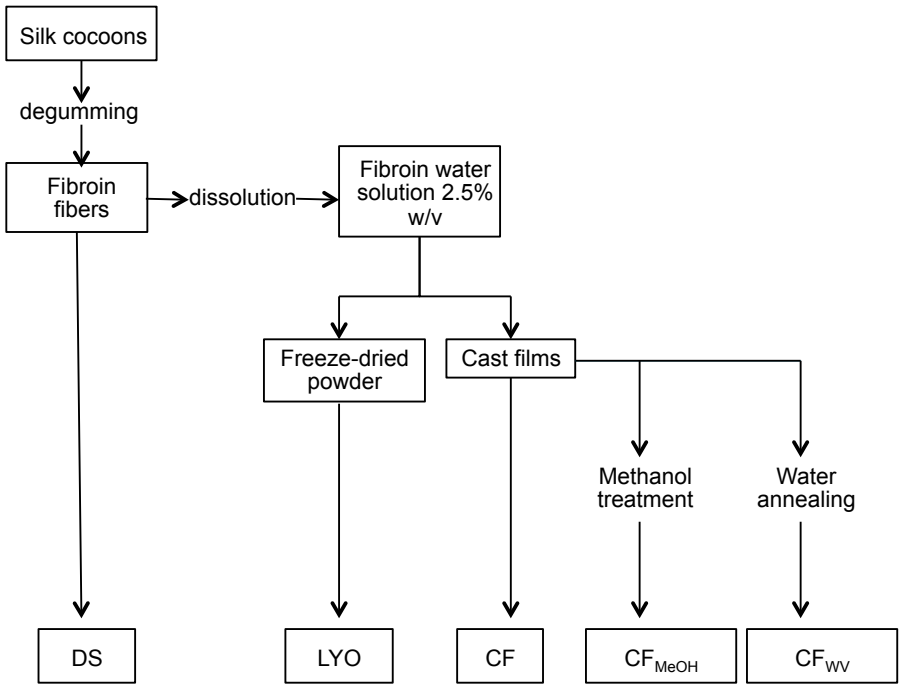

Figure 1: Scheme of protocols used to obtain the different samples starting from silk cocoons: degumming, dissolution, freeze-drying, stabilization methods, and sample codes.

2.4 Samples characterization.

2.4.1 *Infrared spectroscopy analysis.* Protein secondary structures were determined by Fourier transform infrared spectroscopy (FTIR) in attenuate total reflectance (ATR) mode, through a Perkin Elmer Spectrum One Spectrophotometer (Perking Elmer, Waltham, MA, U.S.A.) equipped with Zinc Selenide crystal on ATR. Samples were analysed in dry condition, placed in FTIR sampling surface and compressed until a minimum force of 100N was reached. Sample spectra were averaged over 64 scans, ranging from 650 cm^{-1} to 4000 cm^{-1} at a resolution of 4 cm^{-1}.

2.4.2 *Thermal analysis.* Thermal analysis was conducted on a Differential Scanning Calorimeter Mettler DSC 30 in nitrogen atmosphere with a heating rate of 10 °C/min using standard aluminium pans, in the temperature range 30 °C ~ 350 °C. The glass transition (T_g) and degradation temperatures (T_m) and specific endothermic heat (ΔH) of each silk fibroin sample were determined.

2.4.3 *Solid state nuclear magnetic resonance (NMR) analysis*. ^{13}C cross-polarization under magic angle spinning (CPMAS) measurements were carried out with a Bruker Avance 400WB spectrometer operating at a proton frequency of 400.13 MHz equipped with a double resonance

wide bore MAS probe. In order to quantify the secondary structures formed with the different processing of the samples, the CPMAS experimental conditions were deduced by the study of the cross polarization kinetics for the different flexible and rigid components, since generally the less mobile components cross – polarize better than more mobile ones and this could negatively affect the possibility of obtaining quantitative results from the ^{13}C CPMAS spectra. Accordingly, ^{13}C single pulse MAS experiments with different recycle times and ^{13}C variable contact time CPMAS experiments on the samples were recorded (data not shown) and the quantitative results obtained by the profile fitting of the NMR signals were compared. Considering the good agreement between MAS and CPMAS results and the long duration of MAS experiments, the following conditions were selected for ^{13}C CPMAS spectra acquisition: 100.48 MHz, 5 μs 90° pulse length, 2 ms contact time, 6.3 μs decoupling length, 5 s recycle delay and 4k scans. Samples as fibre, powder or in the form of rolled thin film slices were packed in 4 mm (outer diameter) zirconia rotors, which were spun at 7 kHz under airflow. Adamantane (δ_{CH2} 38.5) was used as external secondary reference.[36] Lineshape analysis was done with Topspin 1.3 Bruker software.

3. RESULTS

3.1 FTIR. The protein structure and the effect of different processing methods on sample conformation were evaluated by infrared spectroscopy (Figure 2). The amide I and amide II bands for the native fibroin fibers (degummed silk) (DS) showed a strong and sharp peak at 1623 cm^{-1} and 1517 cm^{-1} respectively, which are typical regions for β-sheet conformation[15]. Shoulder at 1690 cm^{-1} suggested that this β form is of the antiparallel type[49]. Amide II peak centered at 1527 cm^{-1} and Amide III peak centered at 1234 cm^{-1} with a shoulder at 1265 cm^{-1} confirmed β-

sheet is the main secondary conformation in the natural degummed fiber[50]. On the contrary, after dissolution and freeze-drying (sample LYO), the protein structure underwent conformational transitions as can be seen in the FTIR curve (Figure 2). Adsorption frequencies at 1647 cm^{-1} (Amide I), 1540 cm^{-1} (Amide II), and 1241 cm^{-1} (Amide III) were clearly resolved.[12] Peaks were broader and shifted at higher wavelength if compared with degummed silk (DS), and shoulders at 1690 cm^{-1} and 1265 cm^{-1} were not evident on this curve. On the basis of literature data[15,18], these spectral features are generally ascribed to random coil as main secondary conformation in the protein. However, according to Chen et al.[44] they could be the result of different intermolecular interactions due to protein folding.

Curves related to samples CF, CF_{WV}, and CF_{MeOH} showed a progressive increasing in helices, β-sheet and other secondary beta conformations, such as beta turns and bends. Amide I peak progressively shifted from random coil at 1644 cm^{-1} (CF), to β-structure at 1623 cm^{-1} (CF_{MeOH}). Interestingly, sample CF_{WV} showed an Amide I peak with a double signal at 1653 cm^{-1} and 1623 cm^{-1}, suggesting the co-presence of a two main conformations, beta structure and the three-fold helix or silk III.[51] Amide II peaks became sharper and mainly centered on 1520 cm^{-1} frequency, so progressively excluding signal at 1538 cm^{-1} consistent with a structural transition from an amorphous or a silk I-like type structure to beta conformations[15] (CF_{MeOH}). Shoulder at 1265 cm^{-1} (Amide III silk II form[52]) became evident again just in the sample CF_{MeOH}. To confirm the structural transition due to the fibroin processing, a shoulder at 1700 cm^{-1}, was evident just in the natural degummed fiber (DS) and in the film treated with methanol (CF_{MeOH}), confirming the presence of anti-parallel beta structures.

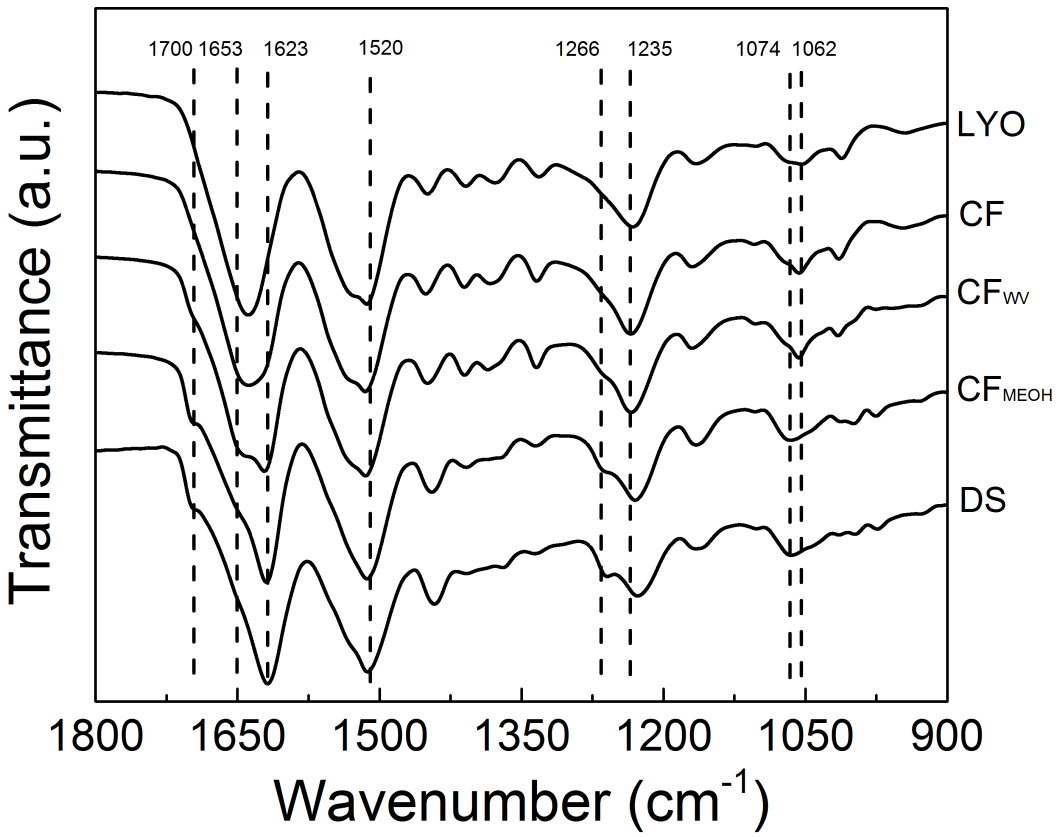

Figure 2: FTIR-ATR curves of fibroin samples: LYO: freeze-dried fibroin water solution; CF: fibroin film after casting; CF_{WV}: fibroin film water annealed; CF_{MeOH}: fibroin film treated in methanol 80% water solution; DS: natural degummed fiber. Dots lines indicated the frequencies of interest discussed in the text.

3.2 Thermal analysis: DSC

DSC curves of all the samples are reported in Figure 3, and the related heat flow values are summarized in Table 1. Natural degummed fiber (DS) displayed two endothermic peaks, the first wide peak (T_e: water evaporation temperature) is centered at about 90°C (total enthalpy 163.4 $J \cdot g^{-1}$), related to the bound water evaporation; and the second sharper one is centered at 311°C

(277 $J \cdot g^{-1}$), related to the thermal degradation of the native protein, respectively. No clear glass transition can be detected in the total heat flow. LYO curve displayed the peak related to water loss centered at lower temperature and broader (associated energy 208 J·g-1) with a contemporary slight shift to higher temperature (110 °C), ~~a~~ decreasing of degradation temperature (290 °C) and the peak area related to silk fibroin degradation (140.5 $J \cdot g^{-1}$) as well. In addition, the degradation peak showed a shoulder at 285 °C. An exothermic peak at 226 °C (ΔH = 19.4 $J \cdot g^{-1}$), and a clear glass transition (179 °C) were also detected. DSC conducted on sample CF, film as cast, showed a slight decrease of the endothermic peaks and associated peak areas, and similar T_g. An exothermic peak was instead detected at lower Temperature (220°C), with a reduced ΔH (14.6 $J \cdot g^{-1}$). The CF_{WV} and CF_{MeOH} films after stabilization treatment showed in general just two endothermic peaks, at 95.6°C and 280°C and 97.7°C and 285°C respectively with similar associated peak areas. In both samples a sensible shift of the degradation peaks at lower temperature was observed with respect to DS. Contemporarily, the exothermic peak was not detected anymore, as well as the glass transition temperature. CF_{WV} sample degradation peak showed a shoulder at 265 °C not visible in the CF_{MeOH} curve, which could suggest the degradation of insoluble helixes structures in the sample.

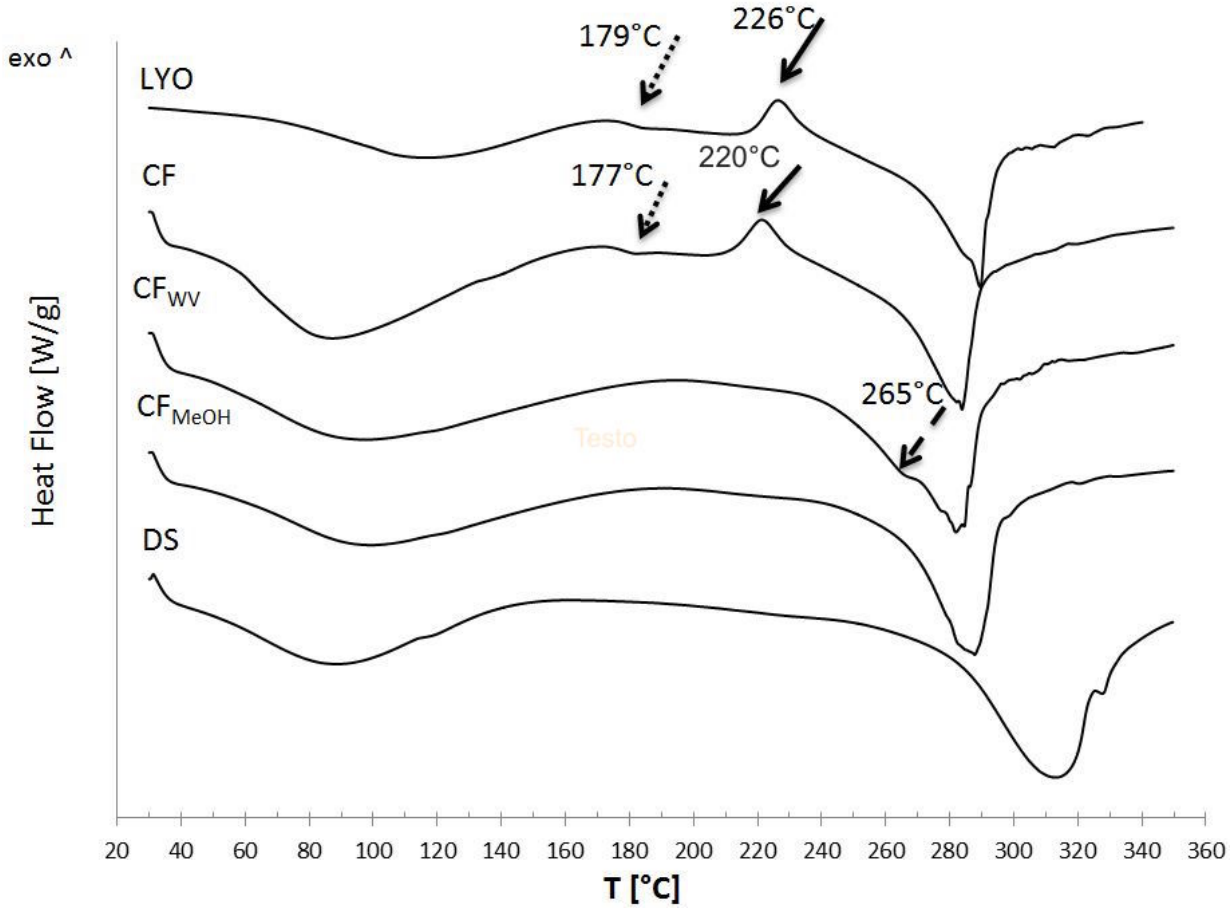

Figure 3. DSC curves of silk fibroin samples obtained by using different protocols. LYO: freeze-dried fibroin water solution; CF: untreated fibroin cast film; CF_{WV}: Fibroin film water annealed after casting; CF_{MeOH}: Fibroin film methanol-treated after casting; DS: degummed silk fiber. Arrows indicate temperatures discussed in the text: crystallization temperature (solid line), T_g (dotted lines), degradation temperature (dashed line).

Sample code	T_e/°C	ΔH_e - J/g^{-1}	T_g/°C	T_c/°C	ΔH_c - J/g^{-1}	T_d/°C	ΔD - J/g^{-1}
LYO	110	208	179	226	19.4	290	140.5
CF	86	195	177.7	220	14.6	280	141.3
CF_{WV}	95.6	155.8	nd	------	-----	280	146.4
CF_{MeOH}	97.7	157.3	nd	-----	-----	285.7	157.4
DS	87.6	163.4	nd	-----	-----	311.1	277

Table 1. Heat flow of silk fibroin samples after DSC analysis (10°C/min). T_e: temperature of endothermal peak; ΔH_e: enthalpy of endothermal peak; T_g: glass-transition temperature; ΔC_p: heat capacity variation at T_g; T_c: temperature of crystallization peak; ΔH_c: enthalpy of crystallization peak; Nd: not detected; -----: not present.

3.3 NMR study. The ^{13}C CPMAS NMR spectra of the prepared samples are shown in Figure 4, and the main signals and their assignments are presented in Table 2. The main signals are also highlighted in the Figure 4, in agreement with the labeling of carbon atoms in the fibroin main aminoacids (displayed in the scheme included in the figure 4). The identified signals confirm the presence of Ala, Gly, Ser and Tyr aminoacids in the protein sequence. According to the literature,[36,53] the carbon atoms of Ala and Gly (C1, C7, C8 and C9), the -CH_2 of Ser (C5) and the aromatic carbons of Tyr (C2, C3 and C4) can be undoubtedly recognized, as summarized in Table 2. Tyr Cβ (δ around 36 ppm) is masked by the noise. Tyr and Ser C=O give very small contribution to peak **1**.

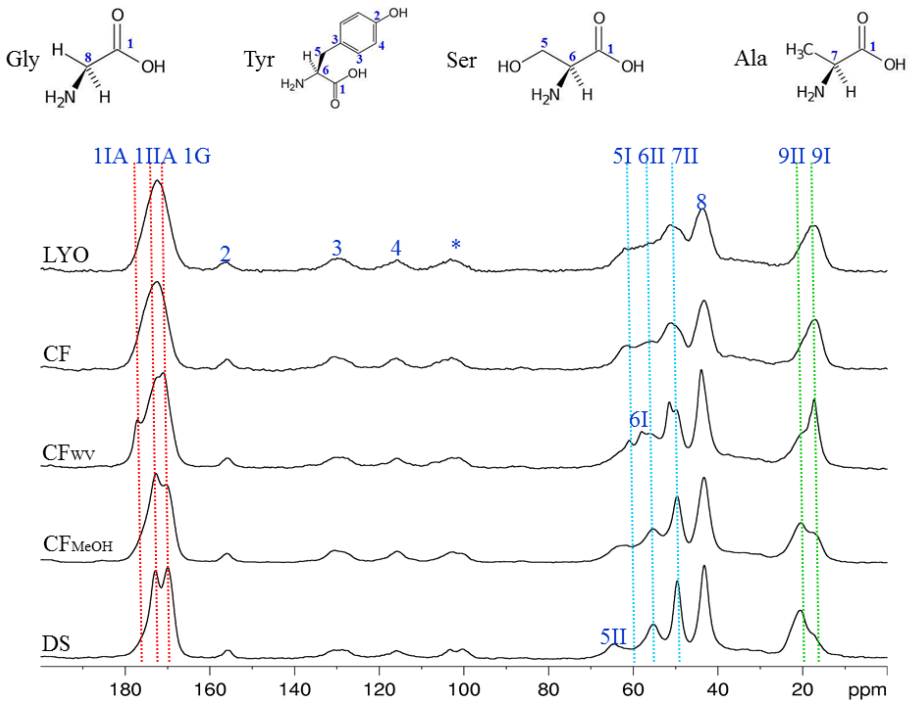

Figure 4. ^{13}C CPMAS NMR spectra of regenerated fibroin samples. Peak assignment and reference molecular structures are reported above. Spinning sidebands are marked with *. Vertical dashed lines are a guide to the eye. The labeling nI (n=1-9) refers to a C atom in a silk I-like/random coil configuration, whereas nII refers to a C atom in a silk II configuration.

C labeling	δ (ppm)	Functional group	component	
$1I_A$	175.8	C=O	Ala	Silk I-like/rc
$1II_A$	172.7	C=O	Ala/(Ser/Tyr)	Silk II
1_G	170.0	C=O	Gly	-
2	155.5	Cξ	Tyr	-
3	131.0	Cγ/Cδ	Tyr	-
4	116.6	Cε	Tyr	-
5II	64.5	Cβ	Ser	Silk II
5I	61.9	Cβ	Ser	Silk I-like/rc
6I	58.0	Cα	Ser	Silk I-like/rc
6II	55.3	Cα	Ser/(Tyr)	Silk II
7I	51.5	Cα	Ala	Silk I-like/rc
7II	49.6	Cα	Ala	Silk II
8	43.8	Cα	Gly	-
9II	20.6	Cβ	Ala	Silk II
9I	17.3	Cβ	Ala	Silk I-like/rc

Table 2. ^{13}C NMR chemical shifts and assignments.[21, 22, 34, 54] The assignments in parenthesis indicate the minor contribution. *rc* refers to random coil.

It is worth of note that the experimental traces of Figure 4 appear different in terms of peak position and line-shape, giving rise to two types of spectra. To the first type belong the lyophilized sample and the cast film (LYO, CF), which are characterized by large and non-resolved signals. The second type includes the degummed silk (DS) displaying sharp and mainly single resolved peaks and the fibroins films post-treated after casting (CF_{MeOH}, CF_{WV}), which show splitting of some sharp peaks with slight variation of chemical shifts. As the source fibroin is the same, the aminoacidic sequence should not change among the samples. Consequently, the sharpness and intensity of the various peaks should be affected only by the conformation of the induced secondary structures.[33, 34]

In solid state NMR, random coil and silk I structures give rise to identical chemical shift[55], therefore they cannot be distinguished on the basis of signal position. Thus, for the sake of simplicity, in Table 2 and Figure 4 we used the labels I and II for the two resonances referred to

silk I/silk I-like/random coils and silk II secondary structures, respectively. The vertical dotted lines in Figure 4 highlight the two contributions to the signals.

As previously noted, the fiber and the post-cured films give rise to spectra with sharper peaks than LYO and CF samples, and this evidence can relate to higher crystallinity or lateral chain mobility in DS, CF_{MeOH} and CF_{WV} samples. The peak **8** (δ 43.8 ppm, Gly Cα) is representative of this behavior and shows a clear change in line-width (LW) among the different samples. We chose to analyze this signal because it is a single well-resolved peak with high signal-to-noise ratio. According to the peak-profile fitting, the full width at half height (FWHH) increases from DS (271.2 Hz) to CF_{WV} (297.8 Hz) and CF_{MeOH} (335.6 Hz).). A larger increase in LW is found for CF and LYO samples with calculated values of 394.0 and 493.9 Hz, respectively.

The LW trend of the other peaks is not so clear. For instance, the aromatic carbons display broad peaks with low signal-to-noise ratio (S/N), and a LW trend is not easily recognizable. The plots relating the LW of peak **8** and the values calculated for other signals show clear correlation only with peaks **7I**, **7II**, **1IA**, **1IIA** and **1G** (Figure 5). The lack of correlation in other cases, due to the significant peak overlapping and the low signal-to-noise ratio, will result in relevant sources of error.

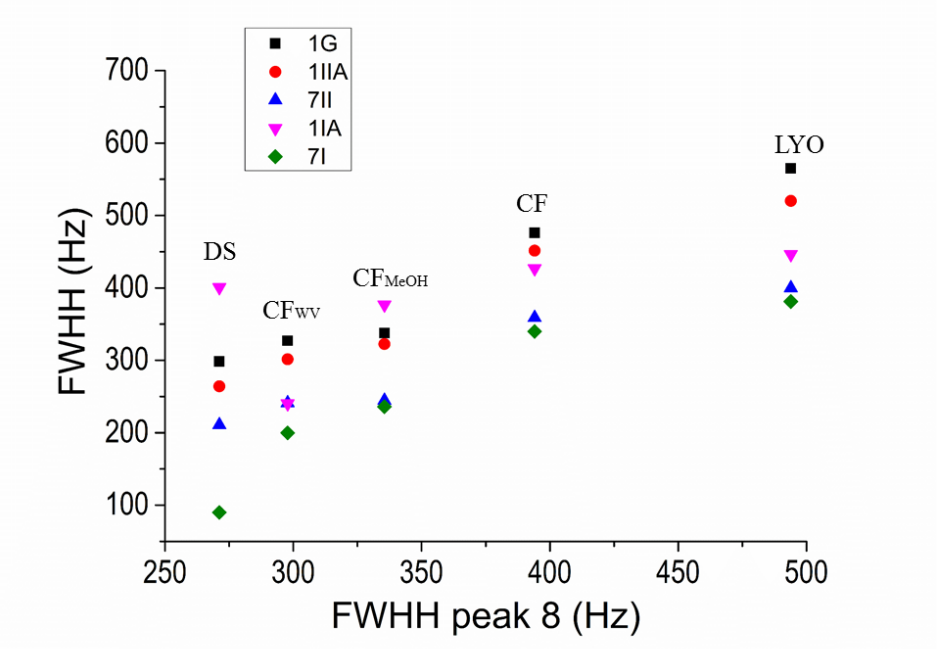

Figure 5. Correlations of full widths at half height (FWHH) of components **8** and **7I**, **7II**, **1IA**, **1IIA** and **1G.**

The linewidth analysis is not capable to definitely discriminate between Silk I-like/random coil and Silk II contributions, since LW values are affected by a variety of parameters.

As reported in the literature,[19,25,30,32,35,38,56,57] the Ala Cβ peak (**9**) is sensitive to the influence of the secondary structure and, consequently, it can be assumed as a diagnostic peak, taking advantage of its position along the peptide chain. According to the DFT study made by Zhou, who calculated Ala Cβ chemical shifts in the main amino acids sequence GAGAGS of silk fibroin in regenerated fibroin film obtained from different solutions,[58] the signal **9** can derive from the overlapping of components at 15.0 ± 0.5, 17.0 ± 0.5, 20.0 ± 0.5, 21.5 ± 0.5 ppm. These four components are assigned to helix-like, helix/random coil, β-sheet and β-sheet-like conformations, respectively. ~~Hence~~ Following the theoretical study of Zhou[58], the profile fittings

of signal **9** of the different samples were calculated using the above reported components, and the results are shown in Table 3.

δ (ppm)	**14.7**	**17.1**	**20.2**	**22.5**	**%Silk II TOT**
LYO	4.0	59.5	19.9	16.6	36.5
CF	3.9	60.8	28.4	6.9	35.3
CF_{WV}	9.0	34.1	49.7	7.1	56.9
CF_{MeOH}	5.0	38.5	36.6	19.9	56.5
DS	9.8	14.7	63.3	12.2	75.5
	helix-like	helix/random coil	β-sheet	β-sheet-like	
	Silk I-like/rc		Silk II		

Table 3. Ala Cβ chemical shifts and calculated relative amounts according to secondary structures with a confidence level of 5% (from peak **9** profile fitting)

By summing peak areas at 14.7 and 17.1 ppm, and peak areas at 20.2 and 22.5 ppm, the contribution of Silk I-like/rc (peak **9I**) and silk II (peak **9II**) can be evaluated, respectively. From the data of Table 3, it appears that the helix/random coil structure is prevalent in casted and lyophilized samples, whereas the β-sheet structure is predominant in post-treated films and degummed silk fiber, with an almost identical amount of silk II in CF_{WV} and in $CF_{MeOH,}$ despite the clear difference in peak **9** line-shape observable in the spectra of Figure 4.

We applied the deconvolution approach also to the analysis of the other resonances, which clearly show the splitting in two components assigned to Silk I-like/rc and Silk II, according to the literature. Thus, for each resonance (peaks **1**, **5**, **6** and **7**), the relative amount of the two components was calculated through the peak-profile fitting. The peak areas corresponding to Silk II contribution of all the considered signals were plotted vs. the Silk II component of peak **9** of the corresponding sample (Figure 6).

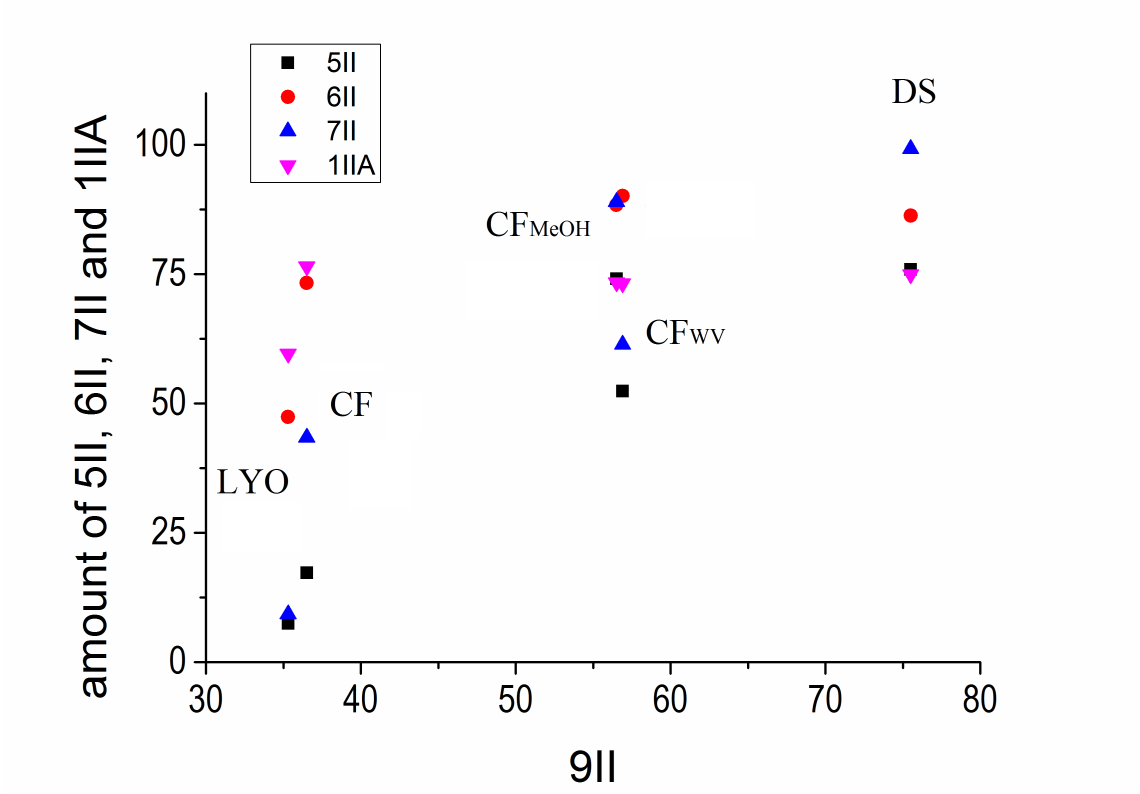

Figure 6. Correlation of amount of component **II** among peaks **1**, **5**, **6**, **7** and **9**.

On the basis of these results, it appears that all the peaks attributed to silk II conformation present a higher amount in DS, CF_{WV} and CF_{MeOH} and a lower presence in CF and LYO samples. Thus, the proposed correlation plot strengthens the structural discrimination. Moreover, the trend of Figure 6 confirms the line-width evolution presented in Figure 5, also suggesting a relation between Silk II amount and peak broadening.

4. DISCUSSION

Regenerated silk fibroin can assume silk I-like and silk II conformations depending on the processing conditions. Regenerated fibroin can also assume intermediate beta structures, like beta turns and beta bends, plus insoluble threefold helical silk III conformation observed at the

water-air interface.[59] Changing in protein secondary conformation and, as a consequence, changing in 3-D self-assembling of the molecule strongly affect material properties such as bound water content, stability, degradation kinetic, and also the biological performance.[42,60,61] Here, the secondary conformations of different silk samples were evaluated by FTIR, DSC, and NMR solid-state analysis.

Natural degummed silk fiber (pure fibroin, DS), as expected, showed the highest degree of crystallinity and thermal stability. Amide I, II, and III related to strong anti-parallel beta structures and intermolecular H-bondings were clearly detected by FTIR-ATR analysis (Figure 2). Native fibroin fiber stability, due to high crystallinity, was confirmed by DSC measurements. Glass transition, as well as the crystallization peak, weren't obvious due to the reduced quote of amorphous regions and the degradation temperature shifted at high temperature ($T_d \sim 309°C$) (Figure 3). This picture is in perfect agreement with the features of the ^{13}C NMR spectrum. The peak sharpness confirms the high crystallinity of this sample (Figure 5) and the profile fitting analysis of the selected peak **9** due to Ala Cβ proves that Silk II is the predominant secondary structure (75.5 %, Table 3).

On the opposite side, a remarkable increase of random coil conformation was observed in sample LYO as a consequence of the silk fibroin dissolution process that induces łoss of pristine secondary structure. This can be clearly seen in the FTIR-ATR curve of sample LYO, where the amide I, II and III peaks became broader and shifted to higher wavelength, and shoulder at 1265 cm^{-1} (silk II) was not detected. Conformational changes affect also the thermal behavior of LYO sample. DSC curve showed a small endothermic peak/step at 179 °C due to glass transition

temperature, and also a crystallization peak around 226 °C before degradation, indicating a decrease of crystallinity and thermal stability as well, in the sample if compared with the degummed fiber. Interestingly, the degradation peak of LYO sample showed a shoulder at 285 °C, probably due to degradation of random coil and helices components. This effect becomes more evident in the CF_{WV} sample, where the degradation tended to be more complex, involving thermal degradation of both alpha helix structures (silk I-like and/or silk III), and beta sheet crystals, compared with other beta-conformation dominated samples (DS, CF_{MeOH}). This double peak degradation phenomenon is also consistent with the FTIR data previously discussed. Methanol treated sample, $CF_{MeOH,}$, showed a similar degradation temperature as CF_{WV} without displaying a shoulder at 285°C and a crystallization peak indicating the increase of beta sheet conformation. DSC data were well correlated to the FTIR observations, in particular when comparing the amide I peaks (CF_{WV} showed a peak at 1648cm^{-1}, indicating the alpha helix conformation, which is not present in the CF_{MeOH} spectra). The increasing of beta-intermediate structures as well as helices components, affect material stability in agreement with the observed degradation temperature decreasing.

In agreement with the above discussion based on FTIR and DSC data, the NMR spectrum of LYO sample is broad with linewidth that are twice larger than DS ones. Moreover, the lineshape analysis of peak **9** indicates that about 60% of the structure is random coil. A similar conformation is evidenced for the untreated sample CF that is also characterized by 60% of random coil structure. However, the full width at half height of CF NMR peaks is smaller than that calculated for LYO sample, suggesting a decrease of disorder that is consistent with the calculated 28% of β-sheet structure (Table 3). In agreement with this observation, a broader

peak is also visible for the amide I in FTIR spectra, indicating a starting increasing of alpha helix conformation induced by casting process. The starting conformational transition was even well supported by the change in shape of peak in the range of 1060-1080 cm^{-1}.[61]

The profile fitting analyses of NMR Ala Cβ peak (**9**) performed with the signal components proposed in the theoretical study of Zhou and used in model peptide studies[58] lead to the conclusion that CF_{WV} and CF_{MeOH} samples present a similar conformation mixture (Table 3), despite the qualitative spectra overview and the conclusions of FTIR and DSC data. This fact, together with the knowledge of the possible presence of other conformations related to the water annealing[48] stimulated a deeper inspection of NMR peak line-shapes, and highlighted that additional components should be considered in order to better represent the profile of characteristic peaks of CF_{WV}. Thus, the profile fitting analysis of Ala C_β peak (peak **9**) was run adding one more resonance at 18.2 ppm, which was assigned by Ando et al. to 3_1-helix structures in $(Ala\text{-}Gly)_n$ polypeptides.[62] The use of this signal component for the line-shape analysis of all the other samples fails and this strongly supports the unique behavior of CFWV in our sample set. Figure 7 compares the results of the profile fitting analysis of the Ala C_β peak (peak **9**) of all samples. Despite the low amount of the Silk III-like in CFWV, it is clear from figure 7~~b~~ that the use of an additional component restores the accordance of NMR with both DSC and FTIR results, with a reduced calculated value of Silk II conformation (47.3%). The addition of a new component for CF_{WV} is also in agreement with the appearance in the FTIR spectrum of a vibration at 1648 cm^{-1}, which can be attributed to the three-fold helix (silk III) found at air-water interface, in agreement with Kaplan *et al.*[16] Moreover, it can be justified by the observation of the shoulder at 261°C in the DSC trace, which was absent in the case of CF_{MeOH} curve. The

presence of silk III is also consistent with the processing conditions experienced by the sample; consequently, we propose to assign the NMR component at 18.2 ppm to the insoluble three-fold helix structure. This fact is significant since FTIR method itself usually has drawbacks to separate peaks from the insoluble three-fold helix (silk III) structures (1645~1655 cm^{-1}) to other soluble helical structures (1645~1650 cm^{-1}) and the random coil structures (1640~1645 cm^{-1}). While the NMR method used here can give a clear calculation of the insoluble three-fold helix (silk III) component in silk materials, which help us directly know the impact of three-fold helix component to the silk materials in the future studies.

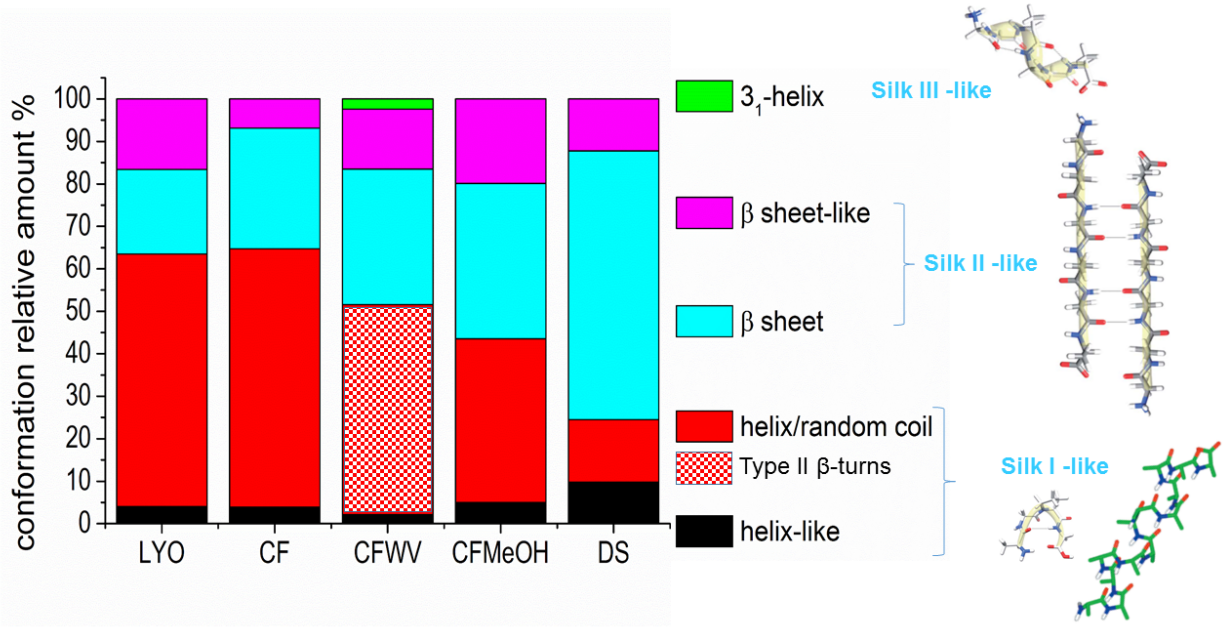

Figure 7. Relative contributions of Silk I, and Silk II and related structures to peak 9 area in the samples. Data derive from Table 3 with the only exception of sample CFWV whose profile fitting takes into account the additional component at 18.2 ppm. For the sake of clarity, the corresponding molecular structures are also reported, adapted in part from T. Asakura, Y. Suzuki, Y. Nakazawa, G. P. Holland and J. L. Yarger, "Elucidating silk structure using solid-state NMR", Soft Matter, 2013, 9, 11440, with permission of The Royal Society of Chemistry. http://dx.doi.org/10.1039/C3SM52187G and adapted with permission from "β-Peptides: From Structure to Function", R. P. Cheng, S. H. Gellman, and W. F. DeGrado, Chemical Reviews 2001 101 (10), 3219-3232 DOI: 10.1021/cr000045i. Copyright (2001) American Chemical Society."

The new profile fitting procedure produces a reduction of linewidth of the other components, particularly in the case of the resonance at 17.1 ppm. This is surprising since this signal is

assigned to helix/random coils conformations characterized by a low order extent. In a similar way, the profile fitting analysis run on peak 1 highlights the presence of a sharp component centered at 177.5 ppm (see Supporting Information). These evidences, displayed only by the sample CF_{WV}, prompt us to assign these two peaks to a structure similar to the Silk I* proposed by Asakura.[56,57] Accordingly, this represents well-ordered regions of the Silk I-like conformation, consisting of repeated type II β-turn units with alternate intra- and inter-molecular hydrogen bonds. Silk I-like conformations were directly formed during the water annealing due to the presence of water molecules that enhance chain mobility of non-crystalline domains. In addition the process is slower if compared with methanol treatment, so allowing sufficient time for chain self-assembly.[18]

Since Silk I* and random coil structures present the same chemical shift of the Ala Cβ peak, the measure of linewidth, together with the presence of the downfield component of peak **1**, appears the only way to distinguish between them. The comparison with the other samples leads to the assignment of random coil configuration to the predominant Ala Cβ component in LYO, CF and CF_{MeOH} samples, underlining again the peculiarity of CF_{WV} sample.

The above assignment clarifies the fact that the line sharpening does not belong to chain mobility or interaction with absorbed water, which is furthermore present in the same amount of sample CF_{MeOH} according to the DSC data, and strengthens the reliability of the quantitative results proposed in figure 7 and Table 4.

As proposed previously[12], the amide I FTIR band was analyzed in a similar way by adding the component related to the presence of silk III in CF_{WV} sample to the three components centered at about 1690, 1651 and 1621 cm^{-1} assigned to turns, random coil and antiparallel β-sheet structures[12], respectively (Table S1, Supporting Information). The additional component was fixed at around 1646 cm^{-1} that is close to the frequency assigned to three-fold helix by Wilson et al.[15] Table 4 reports the comparison between NMR and IR data evaluation, highlighting the substantial agreement of the data and the benefits achievable by using the combined information from both techniques.

% Silk II	DS	CF_{MeOH}	CF_{WV}	CF	LYO
IR	71.4	52.5	41.9	39.8	30.4
NMR	75.5	56.5	47.3	35.3	36.5

Table 4. Amount of Silk II calculated by line shape analysis of NMR peak 9 and IR amide I band, taking into account the additional component related to silk III in CFWV sample. (error bar for each number is less than 5%).

These results highlight the presence, even if in low amount, of the three-fold helix structure in CF_{WV} sample together with a ordered Silk I*-like conformation, and consequently stimulate to the preparation of samples with increased amount of Silk III. Accordingly, work will be undertaken in order to systematically assess the relations between different processing parameters and three-fold helix content, as well as the influence on detected properties of scaffolds.

5. CONCLUSIONS

Fibroin conformation is one of the most important parameters that influences the final protein material three-dimensional self-assembling, water correlation and mechanical properties, which determining different biological outcomes. Various fibroin structures can be induced by properly designing the process. The influence of different processing protocols and stabilization methods on fibroin secondary structures and supermolecular structures were evaluated by the synergic combination of data obtained through solid state NMR and FTIR-ATR spectroscopies, together with DSC analysis. In particular, different conformations such as three-fold helices dominated silk III and Silk I* in different silk materials were analyzed and quantified in this study. The NMR data, corroborated by FTIR, highlighted the unique features of CF_{WV} sample, in which three-fold helices structures can be detected and quantified together with Silk I* conformation, as a consequence of the stabilization treatment performed on cast film. These insights can have important impact on silk fibroin-based materials, helping to elucidate the three-dimensional self-assembling of the molecule under various treatments, which would impact their water correlation and cells' responses in biomedical applications.

ASSOCIATED CONTENT

Profile fitting of both NMR peaks **1** and **9** and the amide I IR band of the CFWV sample together with the quantitative results is supplied as Supporting Information. This material is available free of charge via the Internet at http://pubs.acs.org.

AUTHOR INFORMATION

Corresponding Author

* Phone: 039 0461 282755. Fax: 039 0461 281977. E-mail: Antonella.motta@unitn.it

Author Contributions

The manuscript was written through contributions of all authors. All authors have given approval to the final version of the manuscript.

Notes

The authors declare no competing financial interest.

REFERENCES

(1) Chao, P-HG.; Yodmuang, S.; Wang, X.; Sun, L.; Kaplan, D.L. Vunjak-Novakovic, G. *J.* Silk hydrogel for cartilage tissue engineering. *Biomed. Mater. Res. B Appl. Biomater.* **2010**, *95*, 84–90.

(2) Ghanaati, S.; Orth, C.; Unger, R.E.; et al. Fine-tuning scaffolds for tissue regeneration: effects of formic acid processing on tissue reaction to silk fibroin. *J. Tissue Eng. Regen. Med.* **2010**, *4*, 464–472.

(3) Wang, Y.; Bella, E.; Lee, C.S.D.; et al. The synergistic effects of 3-D porous silk fibroin matrix scaffold properties and hydrodynamic environment in cartilage tissue regeneration. *Biomaterials* **2010**, *31*, 4672–4681.

(4) Unger, R.; Wolf, M.; Peters, K.; Motta, A.; Migliaresi, C.; Kirkpatrick CJ. Growth of human cells on a non-woven silk fibroin net: a potential for use in tissue engineering. *Biomaterials* **2004**, *25*, 1069–1075.

(5) Aoki, H.; Tomita, N.; Morita, Y.; et al. Culture of chondrocytes in fibroin-hydrogel sponge. *Biomed. Mater. Eng*. **2003**, *13*, 309–316.

(6) Foss, C.; Merzari, E.; Migliaresi, C.; Motta, A. Silk Fibroin/Hyaluronic Acid 3D Matrices for Cartilage Tissue Engineering. *Biomacromolecules* **2013**, *14*, 38–47.

(7) Mandal, B.B.; Park, S.H.; Gil, E.S.; Kaplan, D.L. Multilayered silk scaffolds for meniscus tissue engineering. *Biomaterials* **2011**, *32*, 639–651.

(8) Wang, X.; Kluge, J.A.; Leisk, G.G.; Kaplan, D.L. Sonication-induced gelation of silk fibroin for cell encapsulation. *Biomaterials* **2008**, *29*, 1054–1064.

(9) Riccio, M.; Maraldi, T.; Pisciotta, A.; et al. Fibroin scaffold repairs critical-size bone defects in vivo supported by human amniotic fluid and dental pulp stem cells. *Tissue Eng. Part A.* **2012**, *18*, 1006–13.

(10) Inoue, S.; Tanaka, K.; Arisaka, F.; Kimura, S.; Ohtomo, K.; Mizuno, S. Silk Fibroin of Bombyx mori Is Secreted, Assembling a High Molecular Mass Elementary Unit Consisting of H-chain, L-chain, and P25, with a 6:6:1 Molar Ratio*. *J. Biol. Chem*. **2000**, *275*, 40517–40528.

(11) Zhou, C.; Confalonieri, F.; Jacquet, M.; et al. Silk fibroin: Structural implications of a remarkable amino acid sequence. *Proteins* **2001**, *44*, 119-122.

(12) Hu, X.; Kaplan, D.; Cebe, P. Determining Beta-Sheet Crystallinity in Fibrous Proteins by Thermal Analysis and Infrared Spectroscopy. *Macromolecules* **2006**, *39*, 6161–6170.

(13) Trabbic, K.A.; Yager, P. Comparative Structural Characterization of Naturally- and Synthetically-Spun Fibers of Bombyx mori Fibroin. *Macromolecules* **1998**, *31*, 462–471.

(14) Lotz, B.; Gonthier-Vassal, A.; Brack, A.; Magoshi, J. Twisted single crystals of Bombyx mori silk fibroin and related model polypeptides with beta structure. A correlation with the twist of the beta sheets in globular proteins. *J. Mol. Biol.* **1982**, *156*, 345–357.

(15) Wilson, D.; Valluzzi, R.; Kaplan, D. Conformational transitions in model silk peptides. *Biophys. J.* **2000**, *78*, 2690–2701.

(16) Valluzzi, R.; Gido, S.P. The crystal structure of Bombyx mori silk fibroin at the air–water interface. *Biopolymers* **1997**, *42*, 705-717.

(17) Asakura, T.; Suzuki, Y.; Nakazawa, Y.; Yazawa, K.; Holland, G.P.; Yarger, J.L. Stretching-Induced Conformational Transition of the Crystalline and Noncrystalline Domains of 13C-Labeled Bombyx mori Silk Fibroin Monitored by Solid State NMR. *Macromolecules* **2015**, *48*, 5761-5769.

(18) Lu, Q.; Hu, X.; Wang, X.; Kluge, JA; Lu, S.; Cebe, P.; Kaplan, DL. Water-insoluble silk films with silk I structure. *Acta Biomaterialia* **2010**, *6*, 1380-1387.

(19) Asakura, T.; Suzuki, Y., Nakazawa, K.; et al. Silk structure studied with nuclear magnetic resonance. *Prog. Nucl. Magn. Reson. Spectrosc.* **2013**, *69*, 23-68.

(20) Nazakawa, Y.; Asakura, T. High-Resolution 13C CP/MAS NMR Study on Structure and Structural Transition of Antheraea pernyi Silk Fibroin Containing Poly(l-alanine) and Gly-Rich Regions. *Macromolecules* **2002**, *35*, 2393–2400.

(21) Asakura, T.; Murakami T. NMR of silk fibroin. 4. Temperature- and urea-induced helix-coil transitions of the -(Ala)n- sequence in Philosamia cynthia ricini silk fibroin protein monitored by carbon-13 NMR spectroscopy. *Macromolecules* **1985**, *18*, 2614–2619.

(22) Asakura, T.; Watanabe, Y.; Uchida, A.; Minagawa, H. NMR of silk fibroin. Carbon-13 NMR study of the chain dynamics and solution structure of Bombyx mori silk fibroin. *Macromolecules* **1984**, *17*, 1075–1081.

(23) Asakura, T.; Iwadate, M.; Demura, M.; Williamson, M.P. Structural analysis of silk with 13C NMR chemical shift contour plots. *Int. J. Biol. Macromol.* **1999**, *24*, 167–171.

(24) Asakura, T.; Ashida, J.; Yamane, T. A repeated beta-turn structure in poly(Ala-Gly) as a model for silk I of Bombyx mori silk fibroin studied with two-dimensional spin-diffusion NMR under off magic angle spinning and rotational echo double resonance. *J. Molec. Struct.* **2001**, *306*, 291–305.

(25) Ruan, Q-X; Zhou, P. Sodium ion effect on silk fibroin conformation characterized by solid-state NMR and generalized 2D NMR–NMR correlation. *J. Mol. Struct.* **2008**, *883-884*, 85–90.

(26) Nazakawa, Y.; Asakura, T. Heterogeneous exchange behavior of Samia cynthia ricini silk fibroin during helix–coil transition studied with 13C NMR. *FEBS Lett.* **2002**, *529*, 188–192.

(27) Asakura, T; Nakazawa, Y. Structural Analysis of Silk Fibroins using NMR. In: *Modern Magnetic Resonance*. G. A. Webb Ed.; Springer: Dordrecht, The Netherlands, **2008**; Part 1: Applications in Chemistry, Biological and Marine Sciences, pp 101–106.

(28) Asakura, T.; Suzuki, Y.; Nakazawa, Y.; Holland, G.P.; Yarger JL. Elucidating silk structure using solid-state NMR. *Soft Matter* **2013**, *9*, 11440–11450.

(29) Zhong, J.; Ma, M.; Li, W.; et al. Self-assembly of regenerated silk fibroin from random coil nanostructures to antiparallel β-sheet nanostructures. *Biopolymers* **2014,** *101*, 1181-1192.

(30) Asakura T, Sato H, Moro F, Nakazawa Y, Aoki A. Lamellar Structure in Poly(Ala-Gly) Determined by Solid-State NMR and Statistical Mechanical Calculations. *J. Am. Chem. Soc.* **2007**, *129*, 5703–5709.

(31) Asakura, T.; Demura, M.; Date, T.; Miyashita, N.; Ogawa, K.; Williamson, M.P. NMR study of silk I structure of Bombyx mori silk fibroin with 15N- and 13C-NMR chemical shift contour plots. *Biopolymers* **1997**, *41*, 193–203.

(32) Sato, H.; Kizuka, M.; Nakazawa, Y.; Asakura, T. The Influence of Ser and Tyr Residues on the Structure of Bombyx Mori Silk Fibroin Studied Using High-resolution Solid-state 13C NMR Spectroscopy and 13C Selectively Labeled Model Peptides. *Polym. J.* **2008**, *40*, 184–185.

(33) Asakura, T.; Yao, J.; Yamane, T.; Umemura, K.; Ulrich, A.S. Heterogeneous structure of silk fibers from Bombyx mori resolved by ^{13}C solid-state NMR spectroscopy. *J. Am. Chem. Soc.* **2002**, 8794–8795.

(34) Asakura, T.; Suita, K.; Kameda, T.; Afonin, S.; Ulrich, A.S. Structural role of tyrosine in Bombyx mori silk fibroin, studied by solid-state NMR and molecular mechanics on a model peptide prepared as silk I and II. *Magn. Reson. Chem.* **2004**, *42*, 258-266.

(35) Asakura, T.; Yao, J. ^{13}C CP/MAS NMR study on structural heterogeneity in Bombyx mori silk fiber and their generation by stretching. *Protein. Sci.* **2002**, 2706–2713.

(36) Zhang, H.; Li, L-L.; Dai, F-Y.; et al. Preparation and characterization of silk fibroin as a biomaterial with potential for drug delivery. *J. Transl. Med.* **2012**, *10*, 117.

(37) Kishimoto, Y.; Ito, F.; Usami, H.; et al. Nanocomposite of silk fibroin nanofiber and montmorillonite: Fabrication and morphology. *Int. J. Biol. Macromol*. **2013**, *57*, 124–128.

(38) Ji, D.; Deng, Bin, Y.; Zhou, P. Folding process of silk fibroin induced by ferric and ferrous ions. *J. Mol. Struct.* **2009**, *938*, 305–310.

(39) Mathur, A.B.; Tonelli, A.; Rathke, T.; Hudson, S. The dissolution and characterization of Bombyx mori silk fibroin in calcium nitrate-methanol solution and the regeneration of films. B*iopolymers* **1997**, *42*, 61-74.

(40) Tao, W.; Wei, Y-Q.; Li, M-Z. *J.* Condensed Structure of Regenerated Antheraea pernyi Silk Fibroin Porous Materials Prepared by Freeze-dryingFiber Bioeng. *Informatics* **2009**, *2*, 114–119.

(41) Ishida, M.; Asakura, T.; Yokoi, M.; Saiti, H. Solvent- and mechanical-treatment-induced conformational transition of silk fibroins studies by high-resolution solid-state carbon-13 NMR spectroscopy. *Macromolecules* **1990**, *94*, 88–94.

(42) Motta, A.; Maniglio, D.; Migliaresi, C.; et al. Silk Fibroin Processing and Thrombogenic Responses. *J. Biomater. Sci. Polym. Ed.* **2009**, *20*, 1875–1897.

(43) Park, W.H.; Jeong, L.; Yoo, D.; Hudson, S. Effect of chitosan on morphology and conformation of electrospun silk fibroin nanofibers. *Polymer* **2004**, *45*, 7151–7157.

(44) Chen, X.; Shao, Z.; Marinkovic, N.S. Conformation transition kinetics of regenerated Bombyx mori silk fibroin membrane monitored by time-resolved FTIR spectroscopy. *Biophys. Chem*. **2001**, *89*, 25-34.

(45) Kim, E.Y.; Tripathy, N.; Park, J.Y.; et al. Silk fibroin film as an efficient carrier for corneal endothelial cells regeneration. *Macromol. Res.* **2015**, *23*, 189-195.

(46) Amsden, J.J.; Domachuk, P.; Gopinath, A.; et al. You have full text access to this content Rapid Nanoimprinting of Silk Fibroin Films for Biophotonic Applications. *Adv. Mater*. **2010**, *22*, 1746-1749.

(47) Applegate, M.B.; Marelli, B.; Kaplan, D.L.; et al. Determination of multiphoton absorption of silk fibroin using the Z-scan technique. *Opt. Express* **2013**, *21*, 29637-29642.

(48) Valluzzi, R.; Winkler, S.; Wilson, D.; Kaplan, D.L. Silk: molecular organization and control of assembly. *Philos. Trans. R. Soc. Lond. B Biol. Sci.* **2002**, *357*, 165–7.

(49) Iizukat, E.; Yangt, J.T. The disordered and β-conformations of silk fibroin in solution. *Biochemistry* **1968**, *7*, 2218–2228.

(50) Yoshimizu, H.; Asakura, T. Preparation and characterization of silk fibroin powder and its application to enzyme immobilization. *J. Appl. Polym. Sci.* **1990**, *40*, 127–134.

(51) Wilson, D.; Valluzzi, R.; Kaplan, D. Conformational transitions in model silk peptides. *Biophys. J.* **2000**, *78*, 2690-2701.

(52) Magoshi, J.; Magoshi, Y.; Becker, M.A.; Kato, M.; Han, Z. Crystallization of silk fibroin from solution. *Thermochimica Acta* **2000**, *352-353*, 165–169.

(53) Asakura, T.; Sugino, R.; Okumura, T.; Nakazawa, Y. The role of irregular unit, GAAS, on the secondary structure of Bombyx mori silk fibroin studied with 13C CP/MAS NMR and wide-angle X-ray scattering. *Protein Sci.* **2002**, *11*, 1873–1877.

(54) Creager, M.S.; Izdebski, T.; Brooks, A.E.; Lewis, R.V. Elucidating metabolic pathways for amino acid incorporation into dragline spider silk using 13C enrichment and solid state NMR. *Comp. Biochem. Physiol. A Mol. Integr. Physiol.* **2011**, *159*, 219–24.

(55) Asakura, T., Kuzuhara, A., Tabeta, R., and Saito, H. Conformational characterization of Bombyx mori silk fibroin in the solid state by high-frequency carbon-13 cross polarization-magic angle spinning NMR, x-ray diffraction, and infrared spectroscopy. *Macromolecules* **1985**, *18*, 1841-1845.

(56) Asakura, T.; Okushita, K.; Williamson, MP. Analysis of the Structure of Bombyx mori Silk Fibroin by NMR. *Macromolecules* **2015**, *48*, 2345–2357.

(57) Asakura, T.; Sato, Y.; Aoki, A. Stretching-Induced Conformational Transition of the Crystalline and Noncrystalline Domains of 13C-Labeled Bombyx mori Silk Fibroin Monitored by Solid State NMR. *Macromolecules* **2015**, *48*, 5761–5769.

(58) Zhou, P.; Li, G.; Shao, Z.; et al. Structure of Bombyx mori Silk Fibroin Based on the DFT Chemical Shift Calculation. *J. Phys. Chem. B* **2001**, *105*, 12469-12476.

(59) Valluzzi, R.; Gido, S.P.; Muller, W.; Kaplan, D.L. Orientation of silk III at the air-water interface. *Int. J. Biol. Macromol.* **1999**, *24*, 237–242.

(60) Fuchs, S.; Motta, A.; Migliaresi, C.; Kirkpatrick, C.J. Outgrowth endothelial cells isolated and expanded from human peripheral blood progenitor cells as a potential source of

autologous cells for endothelialization of silk fibroin biomaterials*Biomaterials* **2006**, *27*, 5399–5408.

(61) Pritchard, E.M.; Hu, X.; Finley, V.; Kuo, C.K.; Kaplan, D.L. Effect of silk protein processing on drug delivery from silk films. *Macromol. Biosci.* **2013**, *13*, 311–20.

(62) Ando, I.; Kameda, T.; Asakawa, N. Polypeptides, in: *Solid State NMR of Polymers*, Ando I. and Asakura T. Eds; Elsevier Academic Press: Amsterdam, NL **1998**; chapter 22, pp 824 - 852.

Processing influence on molecular assembling and structural conformations in silk fibroin: elucidation by solid state NMR

AUTHOR NAMES. E. Callone[1,3], S. Dire'[1,3], X. Hu[5], and A. Motta[1,2,4]

Table of Contents Graphic